GEOPHYSICS, VOL. 81, NO. 5 (SEPTEMBER-OCTOBER 2016); P. E297–E309, 10 FIGS., 4 TABLES.
10.1190/GEO2015-0715.1

Textural control on the quadrature conductivity of porous media

Qifei Niu[1], Manika Prasad[1], André Revil[2], and Milad Saidian[3]

ABSTRACT

Induced polarization (IP) has been broadly used for environmental and hydrogeological applications and in civil engineering. The IP response of a porous medium without metallic particles (described by its quadrature conductivity or its normalized chargeability) is controlled by the interfacial electrochemistry of the electrical double layer and the pore-space geometry. We use the specific surface per unit pore volume normalized by the formation factor (i.e., S_{por}/F) as the controlling textural parameter for the quadrature conductivity. This relationship is obtained by averaging the surface conductance over the pore volume. A database that contains 76 samples (including porous borosilicate glass, sandstones, and clayey sediments) is used to check the new scaling. In addition to these data, we have conducted new IP measurements on 13 samples from the Middle Bakken Formation corresponding to low-porosity clayey materials. Comparison between the experimental data and our model confirms that the ratio S_{por}/F is the dominant textural parameter describing the quadrature conductivity σ'' of a broad range of porous media. The database was also used to test whether the quadrature conductivity depended either on S_{por}, or the specific surface area S_m, or the ratio $S_m/(F\phi)$ (ϕ being the connected porosity). Although the quadrature conductivity scales with S_{por} and S_m for high-porosity sandstones, these relationships are not appropriate for the low-porosity clayey materials presented in this study. However, experimental data support the dependence of the quadrature conductivity on $S_m/(F\phi)$, a published relationship obtained through the volume averaging approach.

INTRODUCTION

Induced polarization (IP) is a geophysical method that measures the reversible storage of electrical charges in a porous material (Marshall and Madden, 1959; Vinegar and Waxman, 1984). In the past 30 years, it has been widely used for hydrogeological and environmental studies and to characterize geomaterials in civil engineering (for reviews, see Kemna et al., 2012; Revil et al., 2012). The IP response of a porous medium without metallic particles can be quantified by the quadrature conductivity σ'' or the normalized chargeability. The case of dispersed metallic particles is discussed in Revil et al. (2015a, 2015b) and will not be discussed further in this paper. The normalized chargeability is defined as the difference between the high-frequency asymptotic (in-phase) conductivity and the low-frequency asymptotic (in-phase) conductivity. The quadrature conductivity σ'' is the "out-of-phase" component of the complex conductivity $\sigma^* = \sigma' - i\sigma''$, where i denotes the pure imaginary number. Note that according to this definition, the quadrature conductivity is positive in this study. The quadrature conductivity of a porous medium is frequency dependent, and this dependence is closely related to the grain-/pore-size distribution of the material (Leroy et al., 2008; Revil and Florsch, 2010; Revil et al., 2014; Niu and Revil, 2016). The IP response of a porous medium at low frequencies (<500 Hz) is mainly related to the polarization of the electrical double layer (EDL), which forms in the interface between minerals and the pore-filling fluid (Revil, 2012). Sorption of heavy metals and metallic cations with a strong affinity for the mineral surface can substantially decrease the polarization of the material (Vaudelet et al., 2011). Several experimental results have confirmed the dependence of IP measurements on the pore (space) geometry (Weller and Slater, 2015) and the interfacial electrochemistry of the EDL (Lesmes and Frye, 2001).

The interfacial electrochemistry of the EDL is related to the pore-fluid chemistry (Schwarz, 1962; Vaudelet et al., 2011) and the surface mineralogy (Lesmes and Frye, 2001; Revil, 2012). The fluid chemistry includes ion mobility, ionic strength, pH, and pore-water

Manuscript received by the Editor 26 December 2015; revised manuscript received 29 April 2016; published online 18 July 2016.
[1]Colorado School of Mines, Department of Petroleum Engineering, Golden, Colorado, USA. E-mail: qniu@mines.edu; mprasad@mines.edu.
[2]Université Savoie Mont Blanc, ISTerre, CNRS, UMR 5275, Le Bourget du Lac, France. E-mail: andre.revil@univ-smb.fr.
[3]BP America Inc., Houston, Texas, USA. E-mail: milad.saidian@gmail.com.

composition (Revil and Skold, 2011; Skold et al., 2011; Vaudelet et al., 2011). It determines the distribution of the counterions in the EDL that balance the extra charges (called counterions) on the mineral surface. Physically, the interfacial electrochemistry and environmental factors such as temperature can be treated as a lumped microparameter, for example, the specific surface conductance (O'Konski, 1960; Revil and Florsch, 2010) in modeling the IP response of porous media. One example of the IP models is the mechanistic Stern layer polarization model developed by Revil and coworkers (e.g., Leroy and Revil, 2009; Revil, 2012, 2013). The Stern layer describes the inner layer of the EDL, the external layer being the diffuse layer.

The pore geometry can also affect the IP response of a porous medium. One important parameter for the pore geometry is the pore size (or the pore-size distribution). Similar to particle size (Schwarz, 1962), the pore size controls the relaxation time of a porous medium when an alternating electric field is applied (Niu and Revil, 2016). In addition, texture can also affect the IP response of a porous medium. For example, experimental data have shown the specific surface area per unit pore volume S_{por} has a linear correlation with the quadrature conductivity for materials with low formation factors, generally smaller than 100 (Börner, 1992; Weller et al., 2010). Revil (2013) demonstrates that the ratio $S_m/(F\phi)$ controls the quadrature conductivity of a porous medium (i.e., the specific surface area divided by the product of the intrinsic formation factor and the porosity). This dependence was obtained by upscaling the local equations to the scale of a representative elementary volume. Currently, there is a debate regarding what textural parameter controls σ'' of a porous medium (see recent discussions in Revil, 2014; Weller et al., 2014; Volkmann and Klitzsch, 2016).

The IP method has been extensively used to solve hydrogeological and environmental problems. In practice, there is an increased need to quantitatively interpret the IP measurements. It is, therefore, of vital importance to identify the appropriate textural parameter (and its limitations), so that better models can be developed for practical applications. The objective of this study is to theoretically develop a general relationship between the quadrature conductivity and the texture of a porous material. We will volume-average the specific surface conductance over the representative elementary volume of a porous material. To test the relationships that will be developed based on theoretical arguments, we also conduct IP measurements over 13 core samples from the Middle Bakken Formation. These low-porosity core samples have distinct petrophysical properties from existing data sets, and they are therefore useful in deciphering what petrophysical relationship between the quadrature conductivity and the texture is appropriate.

THEORY

We first develop a new general theoretical relationship between the quadrature conductivity and the texture of a porous material. The specific surface conductance, a specific electrochemical parameter of the EDL, will be volume-averaged over a representative elementary volume using two different approaches. The quadrature conductivity (a macroscopic quantity) at the scale of this representative elementary volume will be related to this electrochemical volume-averaged quantity.

Averaging over pore volume

We consider a porous medium characterized by a connected porosity ϕ filled with an electrolyte. In the following, we consider the specific surface conductance Σ_s, which characterizes the excess conductivity over the thickness of the EDL in the vicinity of the mineral surface. The quantity Σ_s is associated with interfacial electrochemistry and is independent of pore geometry. The magnitude of Σ_s is proportional to the mobility of the counterions in the EDL and to the surface charge density of the mineral (Revil, 2012). The effective conductivity of the porous medium σ', i.e., the measured conductivity at laboratory scale, can be obtained by means of perturbation theory. When the pore-water conductivity dominates the overall conductivity and the ratio $\Sigma_s/\sigma_w \ll 1$ plays the role of a perturbation (σ_w denotes the conductivity of the pore water), Johnson et al. (1986) obtain

$$\sigma' = \frac{\sigma_w}{F}\left[1 + \frac{2\Sigma_s}{\sigma_w \Lambda} + \mathrm{O}\left(\frac{\Sigma_s}{\sigma_w \Lambda}\right)^2\right], \tag{1}$$

where the intrinsic formation factor F and the characteristic pore size Λ are defined as (Johnson et al. (1986)

$$\frac{1}{F} = \frac{\int |\mathbf{E}_0(\mathbf{r})|^2 dV_p}{\int |\mathbf{E}_0(\mathbf{r})|^2 dV}, \tag{2}$$

and

$$\frac{2}{\Lambda} = \frac{\int |\mathbf{E}_0(\mathbf{r})|^2 dS}{\int |\mathbf{E}_0(\mathbf{r})|^2 dV_p}. \tag{3}$$

In equations 2 and 3, $\mathbf{E}_0(\mathbf{r})$ is the electric field in the limit $\Sigma_s \to 0$ (i.e., in the absence of EDL). Note that the integrations in denominators of equations 2 and 3 are taken over the whole sample volume V and the pore volume V_p, respectively. The integration in the numerator of equation 3 is taken over the wall of the fluid-mineral interface. If we ignore higher order terms, equation 1 assumes the conductivity from bulk and the surface conductivity are in parallel to each other. When the ratio Σ_s/σ_w becomes larger, this is not the case anymore (see Bernabé and Revil, 1995; Niu et al., 2016), and the effective tortuosity describing the tortuous pathways of the current lines shifts progressively from the tortuosity of the bulk pore space to a surface tortuosity (see also Revil and Glover, 1997).

We first consider a specific type of porous media to obtain an explicit expression of the parameter $2/\Lambda$. We assume that the decrease in the porosity of the material is due to the uniform growth of the solid phase into the pore space. The growth of the solid phase can be viewed as a change in F due to a change in ϕ (Johnson et al., 1986), i.e.,

$$\Delta F = -(dF/d\phi)\phi \frac{S}{V_p}\Delta\varepsilon, \tag{4}$$

where S is the surface area and $\Delta\varepsilon$ is a perturbation of the thickness of the surface layer. Alternatively, it can also be treated as a perturbation in the thickness of the conductive EDL coating the surface of the grains (Johnson et al., 1986); i.e.,

$$\Delta\sigma = -\frac{2\sigma_w}{F\Lambda}\Delta\varepsilon. \tag{5}$$

This yields the following expression for $2/\Lambda$:

$$\frac{2}{\Lambda} = -\frac{d\ \ln(F)}{d\ \ln(\phi)}\frac{S}{V_p}. \tag{6}$$

We empirically relate F to ϕ using Archie's (1942) law

$$\frac{1}{F} = \phi^m, \tag{7}$$

where m (dimensionless) is called the porosity or cementation exponent. Then, equation 6 can be simplified as

$$\frac{2}{\Lambda} = mS_{\text{por}}. \tag{8}$$

We consider now that equation 1 applies to the complex conductivity problem. We consider the specific surface conductance is a complex number, $\Sigma_s^* = \Sigma_s' - i\cdot\Sigma_s''$: The real part corresponds to electromigration in the EDL, whereas its imaginary part is associated with its polarization. If we insert equation 8 in the complex conductivity version of equation 1, the measured quadrature conductivity of the sample can be related to the out-of-phase component of the specific surface conductance Σ_s'' by

$$\sigma'' = \frac{1}{F}\, mS_{\text{por}}\Sigma_s''. \tag{9}$$

Note that the cementation factor m is approximately in the range between 1.5 and 4 (Friedman, 2005). Compared with S_{por} and F, the range of the variation in m is very narrow, and therefore it can be regarded as a constant. Equation 9 is also consistent with the equations developed by Revil et al. (2012), for which the quadrature conductivity is expressed as a function of the ratio Q_v/F, where Q_v denotes the excess of charge per unit pore volume. Because Q_v is proportional to S_{por} (their ratio being the charge per unit surface area of the mineral), the scaling between the quadrature conductivity and S_{por} or Q_v is identical. Because Σ_s^* is only associated with interfacial electrochemistry of the EDL (independent on the pore-space geometry), equation 9 indicates that σ'' is controlled by the textural parameter S_{por}/F. This implication is consistent with some published research. For example, Weller and Slater (2012) show that σ'' is linearly proportional to the parameter S_{por}/F based on the diffuse layer polarization model (Rink and Schopper, 1974) and the Stern layer polarization model (Leroy et al., 2008). The merit of equation 9 is that it provides a definite theoretically justified relationship between S_{por}/F and σ''. Therefore, it allows us to conduct a quantitative comparison of the theory with experimental data, as discussed below.

We now discuss an approximation for the parameter $2/\Lambda$ (equation 3), so that a closed-form expression of the quadrature conductivity σ'' can be obtained. We start from equation 2 by considering Archie's law (equation 7). In equation 7, the term ϕ^m is actually a power function of the ratio of pore volume V_p (variable of integration in the numerator of equation 2) over the volume V (variable of integration in the denominator of equation 2). Following the same treatment, we can assume $2/\Lambda$ in equation 3 is also a power function of the ratio of surface area S over pore volume V_p; i.e.,

$$\frac{2}{\Lambda} = \left(\frac{S}{V_p}\right)^p = S_{\text{por}}^p. \tag{10}$$

Therefore, the quadrature conductivity can be related to S_{por} by

$$\sigma'' = \frac{1}{F}\, S_{\text{por}}^p\ \Sigma_s'', \tag{11}$$

where p is an experimental exponent, which is similar to the cementation exponent in Archie's law. Equation 11 can be treated as the equivalent Archie's law for the quadrature conductivity of porous media. It is worth noting that equation 11 is empirical in nature, although some experimental data have been observed to follow such a power-law relationship (Börner, 1992; Kruschwitz et al., 2010; Weller et al., 2010).

Averaging over solid phase

We derived, above, a general relationship between the quadrature conductivity and the pore-space geometry by averaging the specific surface conductance Σ_s^* over the pore volume. Alternatively, we can also average Σ_s^* over the solid phase V_s by considering Joule dissipation:

$$\Sigma_s^* \int |\mathbf{E}_0(\mathbf{r})|^2 dS = \sigma_s^* \int |\mathbf{E}_0(\mathbf{r})|^2 dV_s, \tag{12}$$

where $\sigma_s^* = \sigma_s' - i\,\sigma_s''$ is the equivalent complex conductivity of the solid phase associated with the EDL (termed as specific surface conductivity). Then, the electrical conductivity of the core sample (still in the high-salinity limit) is

$$\sigma^* = \frac{\sigma_w}{F} + \frac{1}{G}\frac{2\Sigma_s^*}{\Pi}, \tag{13}$$

where G denotes the formation factor of the porous medium after interchanging its solid and pore(fluid) phases and the parameter Π can be regarded as a characteristic particle size, having the following form:

$$\frac{2}{\Pi} = \frac{\int |\mathbf{E}_0(\mathbf{r})|^2 dS}{\int |\mathbf{E}_0(\mathbf{r})|^2 dV_s}. \tag{14}$$

In this study, we call G the reciprocal formation factor. The parameter G can be determined using different theories. For instance, $1/G$ can be approximated using effective medium theory as $m(1-\phi^m)$ if σ is larger than $5(m-1)\sigma_s$ (see Bussian [1983] for the electrical conductivity problem). Note that the integration in the denominator of equation 14 is taken over the volume of the solid phase. Similar to Λ, the characteristic particle size Π would exist in the absence of the EDL, and a determination of Π from one experiment is immediately transferable to another.

It is difficult to derive an analytical form for Π, so we now impose restrictions on the porous medium to simplify the problem. Consider a special case in which the solid phase of the porous medium is the assembly of spheres with the same radius a. We also ignore the influence between the spheres. For this particular porous medium, the effect of the surface conductance is exactly equivalent to the increased conductivity of the sphere, i.e., $2\Sigma_s^*/a$ (Schurr, 1964). This implies the characteristic particle size Π is equal to the radius of the sphere, i.e.,

$$\frac{2}{\Pi} = \frac{2}{a} = \frac{2}{3}\frac{4\pi a^2}{\frac{4}{3}\pi a^3} = \frac{2}{3}\frac{S_a}{V_a} = \frac{2}{3} S_m \rho_g, \tag{15}$$

where S_a and V_a are, respectively, the surface area and volume of the sphere(s) and ρ_g denotes the mass density of the grain (in kg m^{-3}). Accordingly, σ_s^* can then be written as

$$\sigma_s^* = \frac{2}{3} \Sigma_s^* S_m \rho_g. \tag{16}$$

This equation is exactly the same as equation 45 in Revil (2012) if we make some assumptions about the relation between Σ_s^* and the surface charge density/ion mobility. Considering equation 13, the measured quadrature conductivity of the sample at laboratory scale can be written as

$$\sigma'' = \frac{2}{3} \frac{1}{G} S_m \rho_g \Sigma_s''. \tag{17}$$

Indeed, the above equations should also hold for spherical particles with different radii if we apply the superposition principle (however, we will not prove this point here). Equation 17 implies that, for porous media with spherical particles, the controlling textural parameter can also be S_m/G.

DATABASE

In this section, we will present a database that will be used to check the previous relationships. The samples in the database contain porous borosilicate glass, clean and clayey sandstones, and low-porosity (tight) clayey sediments. Among them, porous borosilicate glass and sandstone samples are from published research and the low-porosity clayey samples are new. The new samples are from the Middle Bakken Formation, and they have distinct petrophysical properties (e.g., porosity and mineralogy) from the existing ones. Therefore, the existing data sets can be extended to cover a broader range of porous media, especially regarding their porosity and formation factor.

Existing data sets

Porous borosilicate glass

The data of the porous borosilicate samples are from Volkmann and Klitzsch (2016). The related properties of the samples are summarized in Table 1, which include porosity ϕ, specific surface area S_m, specific surface per unit pore volume S_{por}, quadrature conductivity σ'' at 10 Hz, and formation factor F. In Table 1, S_{por} is calculated based on S_m, ϕ, and the grain density $\rho_s = 2230$ kg m^{-3} (Volkmann and Klitzsch, 2016), and the formation factor F is calculated using Archie's equation (equation 9) with $m = 1.5$ (a good estimate for glass beads, see Table 1 of Friedman, 2005). The conductivity of the NaCl solution σ_w is 3×10^{-4} S m^{-1}. The particles in the borosilicate samples are almost round (see the scanning electron microscopy images in Volkmann et al., 2013), and therefore, they can be regarded as spherical particles. The mean particle size of the 15 samples ranges between 2.81 and 316.2 μm, and S_m, measured by the Brunauer-Emmett-Teller (BET) method, comprises between 0.085 and 1.75 m^2 g^{-1}.

Sandstones

The properties of the sandstone samples are summarized in Table 2. All the 48 samples are collected from Börner and Schön (1991), Börner (1992), Lesmes and Frye (2001), Binley et al. (2005), Weller et al. (2011), and Niu et al. (2016). For some samples, the measured S_{por} is not directly available and was estimated

Table 1. Summary of experimental parameters of the porous borosilicate glass samples. Data are from Volkmann and Klitzsch (2016). The related parameters include porosity ϕ, specific surface area S_m, specific surface per unit pore volume S_{por}, quadrature conductivity at 10 Hz σ'', and formation factor F. The related pore-water conductivity is 3×10^{-4} S m^{-1}. The intrinsic formation factor F is calculated as ϕ^{-m} with $m = 1.5$.

No.	ϕ (−)	S_m (m^2 g^{-1})	S_{por} (μm^{-1})	σ'' (mS m^{-1})	F (−)
1	0.316	0.085	0.409	0.0004	5.619
2	0.302	0.132	0.681	0.0009	6.040
3	0.438	0.351	1.004	0.0011	3.451
4	0.390	0.499	1.745	0.0032	4.113
5	0.525	1.200	2.420	0.0046	2.628
6	0.525	1.201	2.423	0.0048	2.629
7	0.510	1.200	2.565	0.0061	2.742
8	0.405	1.475	4.830	0.0064	3.877
9	0.459	1.475	3.873	0.0076	3.213
10	0.459	1.475	3.876	0.0077	3.215
11	0.514	1.750	3.696	0.0088	2.717
12	0.476	1.748	4.288	0.0096	3.044
13	0.540	1.750	3.329	0.0097	2.523
14	0.460	1.750	4.589	0.0098	3.210
15	0.459	1.747	4.592	0.0103	3.215

Table 2. Summary of the sandstone samples. The related parameters include porosity ϕ, specific surface area S_m, specific surface per unit pore volume S_{por}, quadrature conductivity at 1 Hz σ'', and formation factor F. The pore-water conductivity is close to 0.1 S m^{-1}. This table is adapted from Table 1 in Weller and Slater (2015) by adding data sets from Börner (1992) and Niu et al. (2016).

No.	Sample ID	ϕ (−)	S_m (m^2 g^{-1})	S_{por} (μm^{-1})	σ'' (mS m^{-1})	F (−)	Data source
1	L11a	0.221	0.959	8.959	0.163	9.625[4]	
2	L12a	0.234	1.512	13.120	0.241	8.834[4]	
3	L13a	0.202	2.468	25.842	0.251	11.015[4]	
4	L14r	0.223	4.225	39.013	0.254	9.496[4]	
5	LO1a	0.226	0.194	1.761	0.052	9.308[4]	
6	ND1a	0.231	2.905	25.628	0.294	9.007[4]	
7	ND2a	0.275	1.895	13.236	0.295	6.934[4]	
8	ND3a	0.217	3.263	31.198	0.310	9.893[4]	
9	ND4a	0.214	2.861	27.850	0.235	10.101[4]	
10	RD2r	0.264	0.728	5.379	0.050	7.372[4]	Börner and Schön (1991)
11	ST1a	0.257	0.195	1.490	0.021	7.675[4]	
12	WE1a	0.251	1.078	8.526	0.075	7.952[4]	
13	VS1	0.234	1.517	13.162	0.230	8.834[4]	
14	BH1	0.243	0.265	2.189	0.044	8.348[4]	
15	BH6	0.237	0.197	1.679	0.022	8.667[4]	
16	FS1	0.228	0.015	0.137	0.003	9.185[4]	
17	FS2	0.232	0.014	0.125	0.002	8.949[4]	
18	FS3	0.071	0.003	0.121	0.00172	52.858[4]	
19	FS5	0.054	0.003	0.120	0.00182	79.691[4]	
20	E6	0.198	2.960	31.300	0.294	11.350[4]	
21	E7	0.276	1.950	13.200	0.247	6.890	
22	E10	0.224	4.640	41.600	0.275	17.000	
23	E12	0.259	0.748	5.500	0.063	11.000	
24	E14	0.240	1.310	10.700	0.078	11.100[4]	
25	E17	0.181	0.122	1.440	0.011	13.029	
26	B2	0.194	0.198	2.150	0.018	15.600[4]	Börner (1992)
27	B4	0.232	0.261	2.220	0.044	8.978[4]	
28	R1	0.046	0.809	43.500	0.127	100.376	
29	R3	0.097	1.010	24.700	0.144	45.100	
30	F1	0.214	0.015	0.146	0.003	12.500	
31	F3	0.068	0.004	0.126	0.002	45.100	
32	Berea	0.180	0.737	8.897	0.088	15.9	Lesmes and Frye (2001)
33	HEC16-1	0.356	2.311	11.073	0.240	4.708[4]	
34	HEC18-5	0.265	6.338	46.654	0.374	7.330[4]	
35	HEC18-7	0.256	5.703	43.828	0.352	7.720[4]	
36	HEC7-10	0.317	5.487	31.372	0.457	5.603[4]	
37	p5AVr1	0.285	3.950	26.286	0.631	6.573[4]	
38	p7Vr2	0.276	7.277	50.688	0.680	6.897[4]	
39	p9Vr3	0.343	4.532	22.962	0.464	4.978[4]	Binley et al. (2005)
40	VEC18-2	0.256	5.703	43.828	0.559	7.720[4]	
41	VEC7-2	0.283	5.498	36.841	0.406	6.642[4]	
42	VEC7-4	0.283	4.297	28.796	0.478	6.642[4]	
43	VEG1R2	0.275	6.398	44.656	0.544	6.934[4]	
44	VEG2R1	0.311	3.504	20.603	0.252	5.766[4]	

(*continued*)

from its porosity, specific surface area, and grain density (assuming 2650 kg m^{-3}). When the (intrinsic) formation factor was not available, it was determined from their measured porosity and a constant cementation exponent m of 1.5. Note that we also tried other values for m, and it is shown that the change in m (from 1.5 to 2) did not affect the main conclusions made in this study. In general, the petrophysical properties of the sandstone sample vary considerably, covering a broad range of values. For instance, the porosity ranges from 4.6% to 35.6%, and S_{por} comprises between 0.12 and 50.6 μm^{-1}.

New data set

We conducted IP measurements on 13 samples from Middle Bakken Formation to expand the existing data sets. We chose Middle Bakken samples for the following reasons. First, the samples have a large variety in mineralogy. The most abundant minerals in the samples are carbonate (22.7%–49.4%), followed by silica (13.5%–48.3%). The clay content (mainly illite and smectite) changes between 2.5% and 32.1%. Second, these samples generally have very low porosities (2.9%–9.0%) and quite large specific areas (2.52−11.94 m^2/g; see Table 3) by comparison with existing data sets. These samples, therefore, can extend the existing data sets to cover a wider range of porous media. Third, we try to test the applicability of the existing IP theory in interpreting log data for hydrocarbon exploration because significant producible oil reserves exist within the Bakken Formation.

IP measurement and results

The sample was saturated with an NaCl solution in a vacuum chamber. After saturation, the fluid conductivity was measured and the result is $\sigma_w = 0.18$ S m^{-1}. The resistance and phase shift of the saturated samples were then measured from 0.1 Hz to 10 kHz using the spectral IP instrument described in Zimmermann et al. (2008). We use a four-terminal technique with silver-silver chloride electrodes in the measurement to minimize the influence of the electrode polarization. The measured resistance was converted into in-phase and quadrature conductivities using a geometric factor to account for the sample geometry and the electrode arrangement. The geometric factor was numerically calculated using the finite-element method with the commercial finite-element solver COMSOL Multiphysics. For details of the numerical calculations, one can refer to Jougnot et al. (2010) and Butler and Sinha (2012).

The measured quadrature conductivity σ'' is shown in Figure 1 for all the samples. Only the data in the frequency range between 0.1 and 1000 Hz are shown here, because at higher frequencies, the

Table 2. Summary of the sandstone samples. The related parameters include porosity ϕ, specific surface area S_m, specific surface per unit pore volume S_{por}, quadrature conductivity at 1 Hz σ'', and formation factor F. The pore-water conductivity is close to 0.1 S m^{-1}. This table is adapted from Table 1 in Weller and Slater (2015) by adding data sets from Börner (1992) and Niu et al. (2016). (continued)

No.	Sample ID	ϕ (−)	S_m (m^2 g^{-1})	S_{por} (μm^{-1})	σ'' (mS m^{-1})	F (−)	Data source
45	GR	0.246	3.690	31.33	0.291	9.800	
46	BU3	0.089	1.700	46.24	0.720	68.500	Weller et al. (2011)
47	BU12	0.181	0.780	10.46	0.054	18.000	
48	PS1	0.194	3.49	38.424	0.263	37.26	Niu et al. (2016)

[4]The formation factor F is calculated as ϕ^{-m} with, by default, $m = 1.5$.

Table 3. Summary of experimental parameters of the samples from the Middle Bakken Formation (this work). The related parameters include porosity ϕ, specific surface area S_m, specific surface per unit pore volume S_{por}, quadrature conductivity at 100 Hz σ'', and formation factor F. The associated pore-water conductivity is 0.18 S m^{-1}.

No.	Sample ID	ϕ (−)	S_m (m^2 g^{-1})	S_{por} (μm^{-1})	σ'' (mS m^{-1})	F (−)
1	MB7	0.063	6.802	269.262	0.097	100.435
2	MB11	0.035	5.690	422.187	0.024	303.717
3	MB15	0.040	8.518	546.576	0.047	347.763
4	MB16	0.043	6.140	363.813	0.063	130.831
5	MB18	0.029	3.212	286.778	0.026	153.345
6	MB23	0.042	4.747	285.724	0.084	190.045
7	MB24	0.042	6.904	416.968	0.045	259.118
8	MB40	0.047	2.525	134.795	0.026	272.343
9	MB49	0.071	5.505	190.186	0.042	132.914
10	MB51	0.075	8.531	279.003	0.047	131.766
11	MB52	0.065	5.526	211.136	0.043	77.211
12	MB54	0.071	8.362	289.388	0.060	151.285
13	MB56	0.090	11.944	321.273	0.043	135.368

influence of interfacial/membrane polarization and electromagnetic coupling effect could be significant. It is shown that almost all the samples do not exhibit a clear relaxation peak in σ''. It seems there exists a critical frequency f_c, below which the quadrature conductivity increases monotonically with the frequency. When $f > f_c$, the quadrature conductivity reaches a plateau, and this plateau usually lasts for one or two orders until the membrane/interfacial polarization starts to play important roles. This typical IP response corresponds to the "type A" material as defined in Revil (2013), which is characterized by a broad pore-size distribution. The typical pore-size distribution of the Middle Bakken samples is determined using the mercury injection capillary porosimetry (MICP), and the result is shown in Figure 2. The sample used for MICP was cored from the location near where sample MB23 was cored. As shown in Figure 2, the pore size of the sample is mainly distributed from 0.005 to 0.1 μm. This broad pore-size distribution is associated with a relatively flat quadrature conductivity response (see Revil, 2013). In this sense, the pore-size distribution from MICP is consistent with the IP responses in Figure 1 for the Middle Bakken samples.

Petrophysical properties

The quadrature conductivity of the Middle Bakken samples at 100 Hz is summarized in Table 3. Note that we chose the data at 100 Hz for the Middle Bakken samples instead of data at 1 Hz. This is because we believe the quadrature conductivity at 100 Hz is more appropriate to quantify EDL polarization of these low-porosity clayey samples (to be discussed in detail later). This is due to the small size of the clay particles, which would therefore polarize at higher frequencies. The relevant petrophysical properties, such as porosity, specific surface area, and specific surface per unit pore volume, are shown in Table 3 for the Middle Bakken samples. The porosity was measured by the change in the weight of saturated samples before and after drying. The specific surface area was determined using the BET method. The specific surface per unit pore volume was calculated based on the porosity, specific surface area, and grain density (assuming 2650 kg m^{-3}).

Because the Middle Bakken samples contain a significant amount of clay minerals, the surface conductivity cannot be ignored. To determine the formation factor of the samples, we conduct the electrical conductivity measurement at a second salinity, $\sigma_w = 11.9$ S m^{-1}. At this salinity, the surface conductivity might still have some influences on the overall conductivity, and it may not be appropriate to determine the formation factor as the ratio of $\sigma_w = 11.9$ S m^{-1} over the sample conductivity. Here, we provide a simply way to estimate the (intrinsic) formation factor based on two apparent formation factors. As shown in Niu et al. (2016), the asymptotic behavior of apparent formation factor $F_a(\sigma_w)$ can be related to intrinsic formation factor F and σ_w by

$$F_a = \frac{F\sigma_w}{m(1-1/F)\sigma_s' + \sigma_w}, \tag{18}$$

where σ_s' is the real part of the specific surface conductivity σ_s^*. The apparent formation factor F_a is calculated as the ratio of the fluid conductivity over the measured in-phase conductivity of the samples; i.e., $F_a = \sigma_w/\sigma'$. Note that equation 18 is derived from the differential effective medium theory (Bussian, 1983) using binomial expansion and retaining only first-order terms. A similar relation is also proposed by Weller et al. (2013).

There are only two unknowns in equation 18, i.e., F and $m(1-1/F)\sigma_s'$, and therefore measurements at two salinities are sufficient for the calculation of the (intrinsic) formation factor.

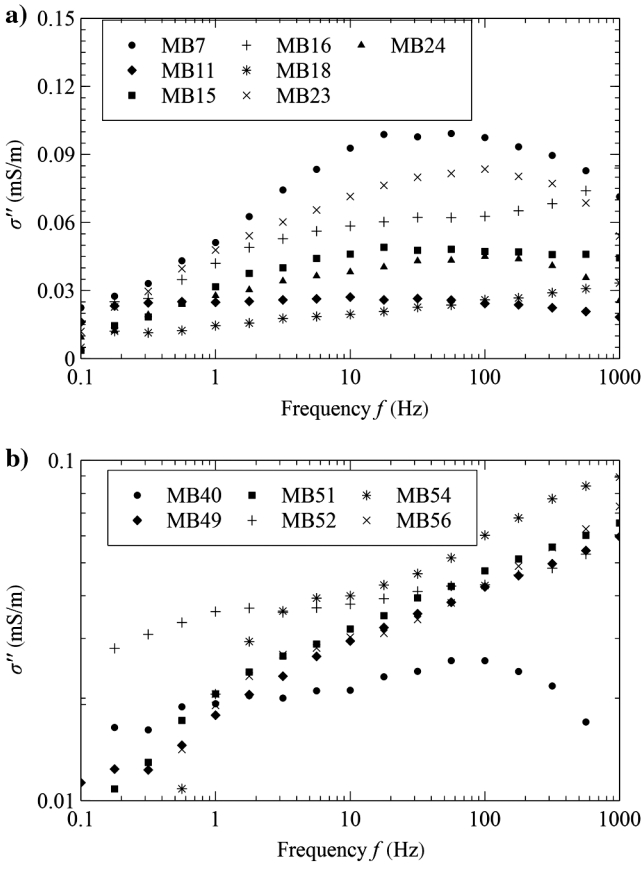

Figure 1. The measured quadrature conductivity σ'' (0.1–1000 Hz) of the Middle Bakken samples. (a) Samples MB7, MB11, MB15, MB16, MB18, MB23, and MB24. (b) Samples MB40, MB49, MB51, MB52, MB54, and MB56. The pore-fluid conductivity σ_w is 0.18 S m^{-1} (NaCl, $T = 22$°C).

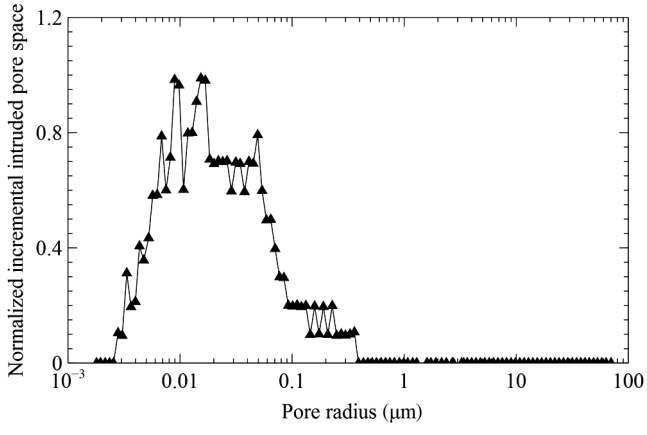

Figure 2. The pore- (throat)-size distribution of a typical Middle Bakken sample obtained from MICP. The sample is cored from the location close to sample MB 23. The pore size is mainly ranging from 0.005 to 0.1 μm.

We use the measured in-phase conductivity at two salinities to calculate F for all the samples using equation 18, and the results are shown in Table 3. In Figure 3, we plot the apparent formation factor (two salinities) against the intrinsic formation factor to demonstrate the influence of the surface conductivity. For $\sigma_w = 11.9$ S m^{-1}, the apparent formation factor is quite close to the intrinsic formation factor, although it could still significantly underestimate the value of F when $F > 300$ (Figure 3). For $\sigma_w = 0.18$ S m^{-1}, the apparent formation factor is considerably lower than the intrinsic formation factor, indicating a very strong influence of the surface conductivity.

THEORY VERSUS EXPERIMENTS

Porous media with spherical particles

The experimental data of the porous borosilicate glass in Table 1 are used to verify equation 9. The quadrature conductivity σ'' multiplied by the formation factor F is plotted against the specific surface per unit pore volume S_{por} in Figure 4. According to equation 9, the product $\sigma'' \cdot F$ is linearly proportional to S_{por} for a specific porous medium and the slope is $m \cdot \Sigma_s''$, which can be related to pore-fluid chemistry and surface mineralogy, based on the Stern layer polarization model (Revil, 2012):

$$\Sigma_S'' = Q_s \beta_{(+)}^S f_p, \tag{19}$$

where Q_s is the charge density on the mineral surface and $\beta_{(+)}^S$ denotes the ion mobility in the Stern layer. The partition coefficient f_p defines the relative fraction of counterions in the Stern layer and is controlled by the fluid chemistry and the mineralogy of the porous medium. For the porous borosilicate glass, because the fluid chemistry is the same for all the samples, the parameter $m \cdot \Sigma_s''$ is a constant. According to equation 9, the data points in Figure 4 are supposed to show a linear relationship. This is exactly the case shown in Figure 4 for the glass beads. The excellent linear correlation ($R^2 = 0.93$) validates the use of the ratio S_{por}/F as the controlling textural parameter for porous media with spherical grains.

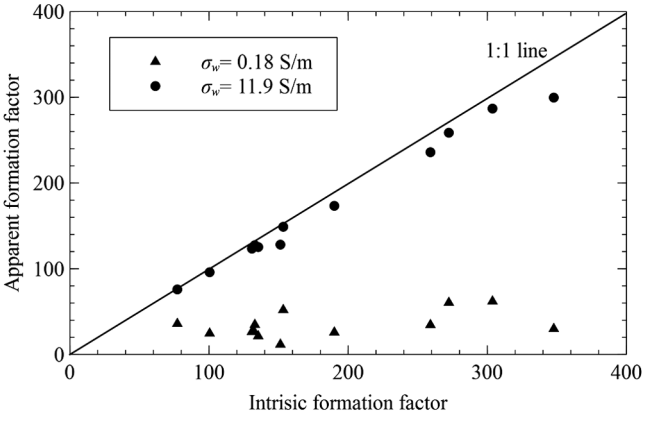

Figure 3. The apparent formation factor (at $\sigma_w = 0.18$ and 11.9 S m^{-1}) versus the intrinsic formation factor of the Middle Bakken samples. The apparent formation factor is determined as the ratio of the fluid conductivity over the measured in-phase conductivity of the sample. The intrinsic formation factor is determined as the asymptotic values of the apparent formation factor at high salinity.

Now, we use the data in Table 1 to test equation 17. The quadrature conductivity σ'' multiplied by the reciprocal formation factor G is plotted against the specific surface area S_m in Figure 5. Note that G is calculated as $m(1-\phi^m)$ according to differential effective medium theory (Bussian, 1983). A strong linear correlation ($R^2 = 0.94$) is found for the porous borosilicate glass, which is consistent with equation 17. The results shown in Figure 5 confirm that the parameter $S_m \cdot G$ can also be the controlling textural parameters for porous media with spherical particles.

Sandstone and low-porosity clayey materials

In Figure 6, the quadrature conductivity σ'' multiplied by the formation factor F is plotted against the specific surface per unit pore volume S_{por} for the sandstone and low-porosity clayey sediment samples in Tables 2 and 3. We believe the low-porosity clayey sediments are distinct from other sediments in the following proper-

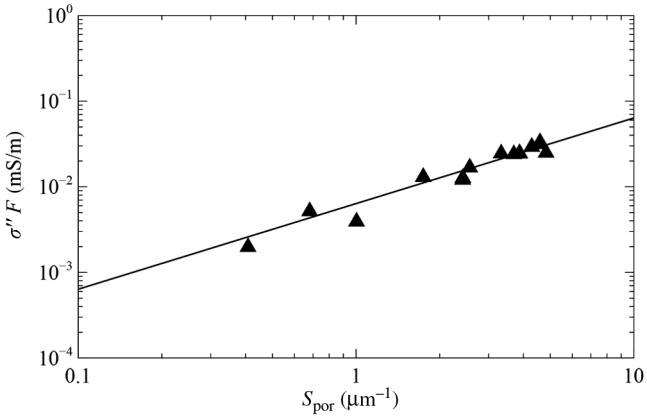

Figure 4. The relation between the quadrature conductivity σ'' multiplied by formation factor F and the specific surface per unit pore volume S_{por} for porous borosilicate samples. The data are from Volkmann and Klitzsch (2016). The solid line is the best linear fit to the data (R^2 is 0.93).

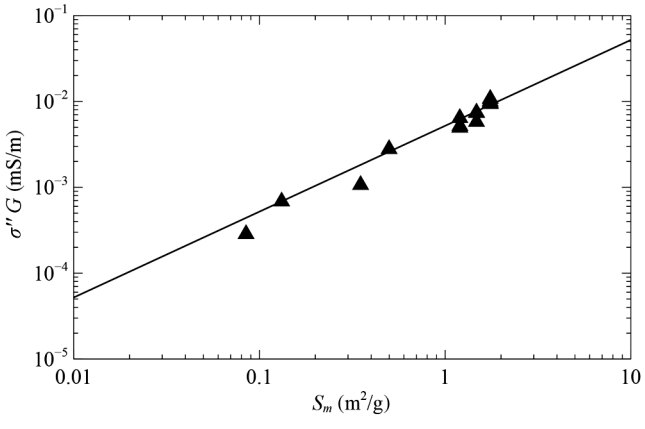

Figure 5. The relation between the quadrature conductivity σ'' multiplied by the reciprocal formation factor G and the specific surface area S_m for porous borosilicate samples. The value of G is calculated as $m(1-\phi^m)$ according to the differential effective medium theory (Bussian, 1983). The data are from Volkmann and Klitzsch (2016). The solid line is the best linear fit to the data ($R^2 = 0.94$).

ties: (1) high specific surface area because of a high clay content and (2) low porosity. For other clayey sandstones, such as sample PS1 in Table 2, although it has large surface area (e.g., 3.49 m^2/g), its porosity is also very large (19.4%). Therefore, the related parameter S_{por} is still lower than the low-porosity clayey sediments as shown in Figure 6. For other low-porosity sandstones, such as sample FS5, although it has very low porosity (e.g., 5.4%), its surface area is also low (0.003 m^2/g), and thus the parameter S_{por} is still very low (e.g., 0.12 μm^{-1}) if compared with Middle Bakken samples as shown in Figure 6. The distinct properties of the low-porosity clayey sediments make Middle Bakken samples a unique material for checking the validation of the existing theory published in the literature and the new theory presented in this study.

The theoretical "clean sand trend" and "clayey sand trend" calculated with equation 8 are also plotted in Figure 6. The clean sand trend is calculated with $Q_s = 0.02$ C m^{-2} (Leroy et al., 2008), $f_p = 0.50$ (Leroy et al., 2008), and $\beta^S_{(+)} = 5.2 \times 10^{-8}$ m^2 V^{-1} s^{-1} (Revil et al., 2014a). The clayey sand trend is calculated with $Q_s = 0.16$ C m^{-2} (Revil et al., 2013), $f_p = 0.95$ (Revil, 2012), and $\beta^S_{(+)} = 1.5 \times 10^{-10}$ m^2 V^{-1} s^{-1} (Revil et al., 2014a). Note that the values of $\beta^S_{(+)}$ of clean and clayey sands are independently derived using the relaxation time and the characteristic pore-size data (Revil et al., 2014a). The different value of $\beta^S_{(+)}$ for clay and sand is justified by the fact that the counterions in the Stern layers are strongly sorbed on the clay mineral surface (van Olphen and Waxman, 1958), but they are only weakly sorbed on the surface of silica (Carroll et al., 2002).

Figure 6 shows that all the low-porosity clayey sediment samples lay close to the theoretical clayey sand trend as predicted by equation 8. However, most of the sandstone samples behave between a clean sand trend and a clayey sand trend. The electrical response of the sandstones is mainly controlled by (1) the amount of clays in the materials and (2) the mineral surface properties. Because clay has higher surface charge density Q_s than other minerals, such as calcite, the amount of clay in a sandstone could dominate its Q_s value, and thus control the specific surface conductance and the quadrature conductivity response. In addition, the contamination of impurity, such as alumina and iron on the grain surface in natural sandstones, could also influence the mineral surface property, and it is possible their surface will exhibit a behavior closer to the clayey sand trend (Revil et al., 2015). An example is the Fontainebleau sandstones. As pointed out by Revil et al. (2014b), the surface properties of the Fontainebleau sandstone are not same as the pure silica, although it is a clean sandstone (99.8% silica). The impurities (Fe and Al) in the silica cement coating the surface of the grains may modify the surface properties of the mineral, and thus have drastic effect on the EDL properties (Ishido and Mizutani, 1981). These two effects explain why the sandstone samples in Figure 6 scatter between the theoretical clean sand trend and clayey sand trend. Despite the scatter in the data, in general, a clear linear relation can still be found in Figure 6 for the sandstones and low-porosity clayey sediments, indicating the validation of S_{por}/F as the controlling textural parameter for the quadrature conductivity.

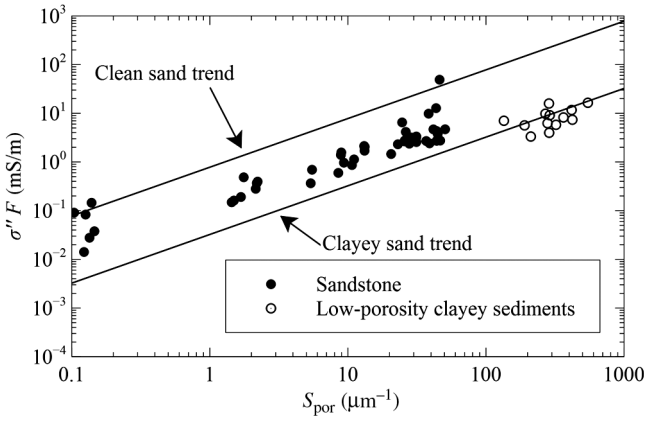

Figure 6. The relation between the quadrature conductivity σ'' multiplied by formation factor F and the specific surface per unit pore volume S_{por} for sandstone and low-porosity clayey sediment samples. The theoretical "clean sand trend" and "clayey sand trend" are also shown in the figure.

TESTING OTHER PARAMETERS

According to the existing IP models, some other textural parameters could also be regarded as the controlling parameter for the quadrature conductivity of porous media. These parameters include S_{por} (see equation 11 in Weller et al., 2011), S_m (see equation 45 in Revil, 2012), and $S_m/(F\phi)$ (see Revil [2013] for detailed discussions or see equation 8 in Revil, 2014). In this section, we use the sandstone and low-porosity clayey sediment samples to test these parameters.

Dependence on S_{por}

The important role of S_{por} in controlling the magnitude of the IP responses has been emphasized in early studies (Börner, 1992; Börner et al., 1996). Recently, Weller and Slater (2015) propose to use S_{por} as the controlling textural parameter based on the experimental fact that σ'' and S_{por} have a single linear relationship for several porous media. We use the data sets in this study to test the statement, and the results are shown in Figure 7, where S_{por} is plotted against σ'' for the samples. Note that the range of S_{por} in Figure 7 is between 0.1 and 100 μm^{-1}, 1 order larger than that in Weller and Slater (2015). In Figure 7, the low-porosity clayey

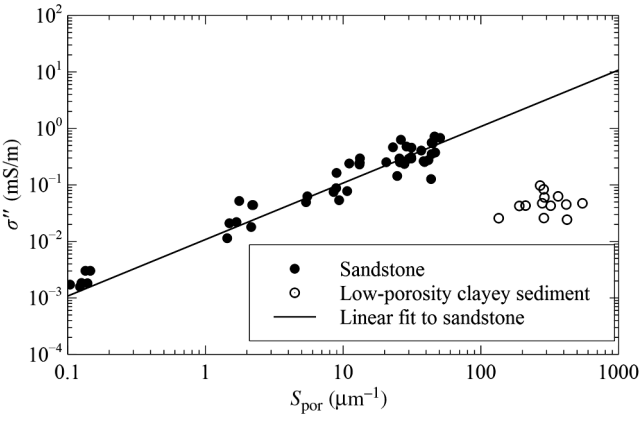

Figure 7. The relation between the quadrature conductivity σ'' and the specific surface per unit volume S_{por} for sandstone and low-porosity clayey sediment samples. The solid line is the best linear fit to the sandstone samples.

samples exhibit a distinct response from the sandstones that follow a single linear trend. It seems that the specific surface per unit volume S_{por} is not the appropriate textural parameter controlling the quadrature conductivity of porous media.

Dependence on S_m

The POLARIS model developed by Revil (2012) for high-porosity materials states a linear relationship between S_m and σ'', implying S_m as the controlling textural parameter. We now test this implication with the data sets in this study. The quadrature conductivity of the samples is plotted against the specific surface area in Figure 8. A strong linear correlation is found for the sandstone samples. However, the low-porosity clayey materials show a different trend. This indicates that S_m might not be the controlling textural parameter for the quadrature conductivity of low-porosity porous media. As discussed by Revil (2013), it requires a correction by the tortuosity of the material.

Dependence on $S_m/(F\phi)$

Using the volume averaging approach, Revil (2013) develops a new IP model for porous media, which relates σ'' to S_m by the following equation:

$$\sigma'' \approx \frac{1}{F\phi}\rho_s f_p \beta^s_{(+)} Q_s S_m. \tag{20}$$

In equation 20, the term $\rho_s f_p \beta^s_{(+)} Q_s$ represents the influence of interfacial electrochemistry, and the term $S_m/(F\phi)$ denotes the pore geometry. Accordingly, the controlling textural parameter is $S_m/(F\phi)$. To test this, we multiply σ'' by F and ϕ for all the sandstones and low-porosity clayey sediments, and the results are plotted against with S_m in Figure 9. In general, a clear linear correlation is found for all the samples, although the low-porosity clayey sediments, which lie close to the theoretical clayey sand trend, show a slightly different trend with the sandstones. The data points of sandstones scatter between the clean sand trend and clayey sand trend, and their response probably are controlled by the amount of clay or properties of mineral surface as discussed before. Comparing Figures 7–9, it appears the correlation between $S_m/(F\phi)$ and σ'' is better than the correlation between S_m (or S_{por}) and σ''.

Comparing Figures 6 and 9, it seems that S_{por}/F and $S_m/(F\phi)$ can be regarded as the controlling textural parameters for the quadrature conductivity of porous media. Indeed, the parameter S_{por}/F can be rewritten as $\rho_s(1-\phi)S_m/(F\phi)$ if we consider $S_{por} = \rho_s(1-\phi)S_m/\phi$. The term $\rho_s(1-\phi)$ is actually the dry density of the porous media ρ. Considering the fact that the density of consolidated sediments varies within a small range (approximately <30%), S_{por}/F and $S_m/(F\phi)$ can therefore be treated as a nearly equivalent quantity, especially for low-porosity core samples.

DISCUSSION

Influence of fluid conductivity

The quadrature conductivity of the low-porosity clayey sediment samples shown in Table 3 is measured with a pore-fluid conductivity σ_w of 0.18 S m^{-1}. However, other data reported in Table 2 are measured at σ_w = approximately 0.1 S m^{-1}. Therefore, it is necessary to discuss the possible influence of this salinity difference. The fluid salinity can affect the measured in-phase and quadrature conductivities through two ways: (1) changing the tortuosity (Niu et al., 2016) and (2) the partition coefficient (Revil, 2012). Because the influence of the latter is minor as shown in Niu et al. (2016), here we only focus on the former factor. The tortuosity change can be well-captured using the following differential effective medium theory-based conductivity model (Bussian, 1983):

$$\sigma^* = \frac{\sigma_w}{F}\left(\frac{1-\sigma_s^*/\sigma_w}{1-\sigma_s^*/\sigma^*}\right)^m. \tag{21}$$

Essentially, σ_s^* is a weak function of the fluid conductivity as the salinity will change the relative fraction of ions in the Stern/diffuse layer (Revil, 2012). However, this influence is very small, and we simply assume it is constant.

We take sample MB56 as an example to estimate the salinity influence on the quadrature conductivity (100 Hz). The related petrophysical properties of sample MB56 is as follows: F = 135 and

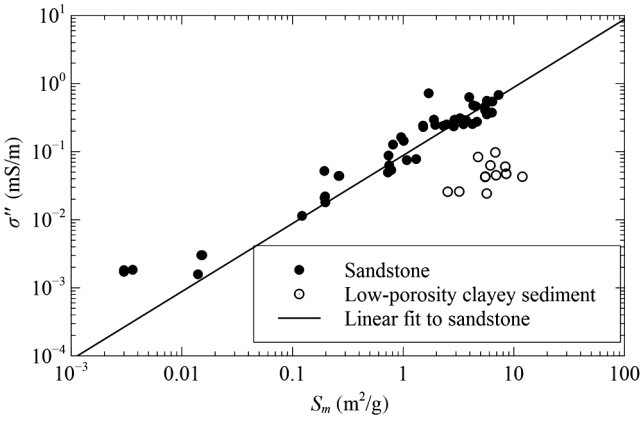

Figure 8. The relation between the quadrature conductivity σ'' and the specific surface area S_m for sandstone and low-porosity clayey sediment core samples. The solid line is the best linear fit to the sandstone samples.

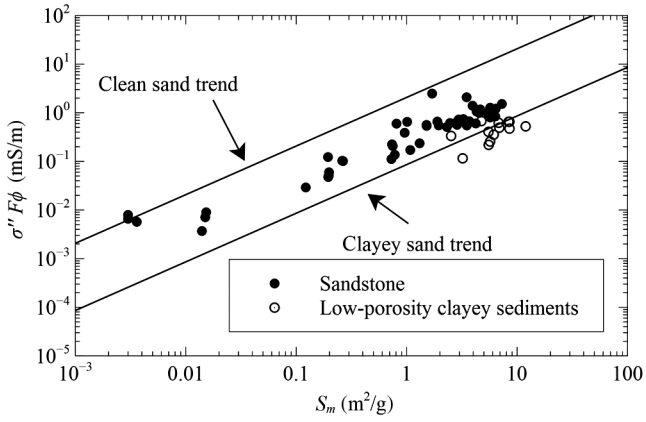

Figure 9. The relation between the quadrature conductivity σ'' multiplied by $F\phi$ (F being the formation factor and ϕ being the porosity) and the specific surface area S_m for sandstone and low-porosity clayey sediment samples. The theoretical clean sand trend and clayey sand trend are also shown in the figure.

$\phi = 0.09$ (resulting in $m = 2.04$). Because there is still an unknown (i.e., σ_s^*), we use the complex conductivity measurements at two salinities to constrain σ_s^*: $\sigma^* = 0.008 + 1.9 \times 10^{-5} i$ S m^{-1} at $\sigma_w =$ 0.18 S m^{-1} and $\sigma^* = 0.09 + 2.9 \times 10^{-5} i$ S m^{-1} at $\sigma_w = 11.9$ S m^{-1}. The determined σ_s^* is equal to $0.004 + 1.6 \times 10^{-5} i$ S m^{-1}, and the theoretical curve and measurements are plotted in Figure 10, which show good agreement. Now, we use equation 21 and the related parameters to estimate the influence of fluid conductivity on the quadrature conductivity of sample MB56. We calculate the quadrature conductivity of the sample at $\sigma_w = 0.1$ S m^{-1}, and the result is 1.84×10^{-5} S m^{-1}, which is very close to the quadrature conductivity at $\sigma_w = 0.18$ S m^{-1} (1.9×10^{-5} S m^{-1}). Note that the difference in the quadrature conductivity is only 3%, indicating that the influence of the difference in the fluid conductivity is insignificant. Therefore, we believe it is appropriate to use the measurements at $\sigma_w = 0.18$ S m^{-1} in this study, and the fluid conductivity difference will not change the conclusion made in the previous sections.

Influence of frequency/pore size

Note that the quadrature conductivity of the Middle Bakken samples in Table 3 is taken at frequency $f = 100$ Hz. We chose this value because at this frequency, the quadrature conductivity of almost all the samples reaches a plateau (see Figure 1), implying a maximum contribution from the EDL polarization. However, data in Table 2 are taken at frequency $f = 1$ Hz, simply following the selection in Börner and Schön (1991) and Börner (1992). The underlying assumption of using $f = 1$ Hz is that the pore size of the materials is intermediate (approximately in the range between 100 and 0.1 μm). This assumption may be valid for sandstones, e.g., for samples in Börner (1992). However, it is questionable to use $f =$ 1 Hz for other materials that are dominated by very small or very large pores.

The characteristic relaxation frequency can be related to the pore size r by using the following equation (Schwarz, 1962):

$$\tau_0 = \frac{r^2}{2D^S_{(+)}}, \tag{22}$$

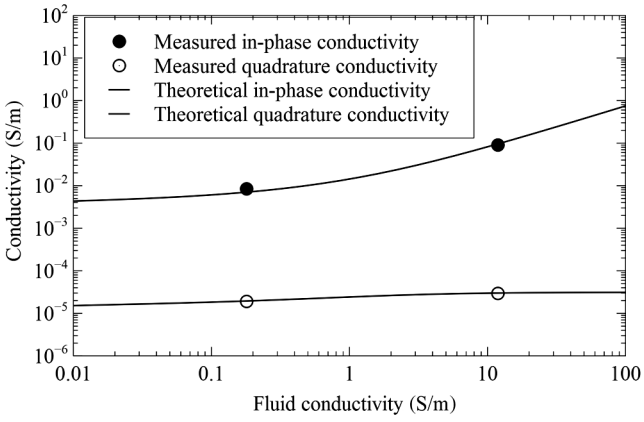

Figure 10. The complex conductivity (100 Hz) of the sample MB56 at different fluid conductivies. Experiments are conducted at $\sigma_w = 0.18$ and 11.9 S m^{-1}. Theoretical curves are calculated using equation 21, and the related parameters are as follows: $F = 135$, $m = 2.04$, and $\sigma_s^* = 0.004 + 1.6 \times 10^{-5} i$ S m^{-1}.

where τ_0 is the characteristic time and $D^S_{(+)}$ is the diffusion coefficient of ions in the Stern layer, which can be related to the mobility of counterions in Stern layer $\beta^S_{(+)}$ through the Nernst-Einstein relationship $D^s_{(+)} = \beta^S_{(+)} T k_b$ for a symmetric monovalent (1:1) electrolyte (such as KCl or NaCl; k_b denotes the Boltzmann constant). As shown in Revil et al. (2014a), the value of $D^S_{(+)}$ is approximately 3.8×10^{-12} m^2 s^{-1} for clayey materials (therefore consistent with $\beta^S_{(+)} = 1.5 \times 10^{-10}$ m^2 V^{-1} s^{-1}) and 1.3×10^{-9} m^2 s^{-1} for clean sand (therefore consistent with $\beta^S_{(+)} = 5.2 \times 10^{-8}$ m^{2}V^{-1}s^{-1}). Now, we use equation 22 to estimate the appropriate relaxation frequency low-porosity clayey samples. The associated pore size is generally smaller than 1 μm (see Figure 2), and therefore, the characteristic relaxation frequency is higher than 10 Hz according to equation 22. To adequately account for the EDL polarization, it is better to choose a higher frequency (e.g., $f = 100$ Hz in this study).

In Weller and Slater (2015), some unconsolidated sediments are used to support their conclusion. However, we did not use the associated data set because the quadrature conductivity data are taken at $f = 1$ Hz. For the unconsolidated sediments, the pore/particle size is quite large, approximately 1 mm (see Slater and Glaser, 2003), and therefore, the associated characteristic relaxation frequency would be very low (approximately <0.01 Hz according to equation 22 using $D^s_{(+)} = 1.3 \times 10^{-9}$ m^2 s^{-1}). Obviously, the use of data at $f = 1$ Hz could underestimate a lot the quadrature conductivity of the samples. Therefore, it is suggested to use low-frequency (<10 mHz) quadrature conductivity data rather than data at 1 Hz for these unconsolidated sediments.

CONCLUSION

A theoretical analysis indicates that the parameter S_{por}/F is the textural parameter controlling the quadrature conductivity of porous media. A database that contains different types of siliciclastic materials has been developed to test this prediction. The comparison between theory and experiments confirms this statement for a broad range of porous media, including borosilicate beads, sandstones, and low-porosity clayey samples. For porous media mainly made of spherical particles, the parameter S_m/G may also be treated as a controlling pore-space geometry parameter. In this case, the reciprocal formation factor G is calculated as $m(1 - \phi^m)$ (m is the cementation exponent entering Archie's law) according to differential effective medium theory. The database is also used to determine the degree of correlation between the quadrature conductivity and S_{por}, S_m (the specific surface area), and the ratio $S_m/(F\phi)$. Although S_{por} and S_m may work for highly porous sandstone core samples, they are not appropriate for the low-porosity clayey sediment samples presented in this study. The experimental data support the parameter $S_m/(F\phi)$, which is obtained using a volume averaging approach as the controlling textural parameter for the quadrature conductivity of porous media.

ACKNOWLEDGMENTS

We thank the Oil Clay Sand and Shale Consortium at the Department of Petroleum Engineering of the Colorado School of Mines for financial support. The work of A. Revil is supported by a grant from LabEx Osug@2020 (investissement d'Avenir — ANR10-

LABX56). We also thank Whiting Petroleum Corporation for providing the core samples. Finally, we thank the four referees and the associate editor for their very useful comments that have significantly improved this manuscript.

REFERENCES

Archie, G. E., 1942, The electrical resistivity log as an aid in determining some reservoir characteristics: Petroleum Transactions of AIME, **146**, 54–62, doi: 10.2118/942054-G.

Bernabé, Y., and A. Revil, 1995, Pore-scale heterogeneity, energy dissipation and the transport properties of rocks: Geophysical Research Letters, **22**, 1529–1532, doi: 10.1029/95GL01418.

Binley, A., L. D. Slater, M. Fukes, and G. Cassiani, 2005, Relationship between spectral induced polarization and hydraulic properties of saturated and unsaturated sandstone: Water Resources Research, **41**, W12417, doi: 10.1029/2005WR004202.

Börner, F. D., 1992, Complex conductivity measurements of reservoir properties: Proceedings of the 3rd European Core Analysis Symposium, 359–386.

Börner, F. D., and J. H. Schön, 1991, A relation between the quadrature component of electrical conductivity and the specific surface area of sedimentary rocks: The Log Analyst, **32**, 612–613.

Börner, F. D., J. R. Schopper, and A. Weller, 1996, Evaluation of transport and storage properties in the soil and groundwater zone from induced polarization measurements: Geophysical Prospecting, **44**, 583–601, doi: 10.1111/gpr.1996.44.issue-4.

Bussian, A., 1983, Electrical conductance in a porous medium: Geophysics, **48**, 1258–1268, doi: 10.1190/1.1441549.

Butler, S. L., and G. Sinha, 2012, Forward modeling of applied geophysics methods using Comsol and comparison with analytical and laboratory analog models: Computers & Geosciences, **42**, 168–176, doi: 10.1016/j.cageo.2011.08.022.

Carroll, S. A., R. S. Maxwell, W. Bourcier, S. Martin, and S. Hulsey, 2002, Evaluation of silica-water surface chemistry using NMR spectroscopy: Geochimica et Cosmochimica Acta, **66**, 913–926, doi: 10.1016/S0016-7037(01)00827-4.

Friedman, S. P., 2005, Soil properties influencing apparent electrical conductivity: A review: Computers and Electronics in Agriculture, **46**, 45–70, doi: 10.1016/j.compag.2004.11.001.

Ishido, T., and H. Mizutani, 1981, Experimental and theoretical basis of electrokinetic phenomena in rock-water systems and its applications to geophysics: Journal of Geophysical Research, **86**, 1763–1775, doi: 10.1029/JB086iB03p01763.

Johnson, D. L., J. Koplik, and L. M. Schwartz, 1986, New pore-size parameter characterizing transport in porous media: Physical Review Letters, **57**, 2564–2567, doi: 10.1103/PhysRevLett.57.2564.

Jougnot, D., A. Ghorbani, A. Revil, P. Leroy, and P. Cosenza, 2010, Spectral induced polarization of partially saturated clay-rocks: A mechanistic approach: Geophysical Journal International, **180**, 210–224, doi: 10.1111/gji.2010.180.issue-1.

Kemna, A., A. Binley, G. Cassiani, E. Niederleithinger, A. Revil, L. Slater, K. H. Williams, A. F. Orozco, F.-H. Haegel, and A. Hoerdt, 2012, An overview of the spectral induced polarization method for near-surface applications: Near Surface Geophysics, **10**, 453–468.

Kruschwitz, S., A. Binley, D. Lesmes, and A. Elshenawy, 2010, Textural controls on low-frequency electrical spectra of porous media: Geophysics, **75**, no. 4, WA113–WA123, doi: 10.1190/1.3479835.

Leroy, P., and A. Revil, 2009, A mechanistic model for the spectral induced polarization of clay materials: Journal of Geophysical Research: Solid Earth, **114**, B10202, doi: 10.1029/2008JB006114.

Leroy, P., A. Revil, A. Kemna, P. Cosenza, and A. Ghorbani, 2008, Complex conductivity of water-saturated packs of glass beads: Journal of Colloid and Interface Science, **321**, 103–117, doi: 10.1016/j.jcis.2007.12.031.

Lesmes, D. P., and K. M. Frye, 2001, Influence of pore fluid chemistry on the complex conductivity and induced polarization responses of Berea sandstone: Journal of Geophysical Research: Solid Earth, **106**, 4079–4090, doi: 10.1029/2000JB900392.

Marshall, D. J., and T. R. Madden, 1959, Induced polarization: A study of its causes: Geophysics, **24**, 790–816, doi: 10.1190/1.1438659.

Niu, Q., and A. Revil, 2016, Connecting complex conductivity spectra to mercury porosimetry of sedimentary rocks: Geophysics, **81**, no. 1, E17–E32, doi: 10.1190/geo2015-0072.1.

Niu, Q., A. Revil, and M. Saidian, 2016, Salinity influence of the complex surface conductivity of Portland sandstone: Geophysics, **81**, no. 2, D125–D140, doi: 10.1190/geo2015-0426.1.

O'Konski, C. T., 1960, Electric properties of macromolecules. V: Theory of ionic polarization in polyelectrolytes: The Journal of Physical Chemistry, **64**, 605–619, doi: 10.1021/j100834a023.

Revil, A., and P. W. J. Glover, 1997, Theory of ionic surface electrical conduction in porous media: Physical Review B, **55**, 1757–1773, doi: 10.1103/PhysRevB.55.1757.

Revil, A., 2012, Spectral induced polarization of shaly sands: Influence of the electrical double layer: Water Resources Research, **48**, W02517, doi: 10.1029/2011WR011260.

Revil, A., 2013, Effective conductivity and permittivity of unsaturated porous materials in the frequency range 1 mHz–1 GHz: Water Resources Research, **49**, 306–327, doi: 10.1029/2012WR012700.

Revil, A., 2014, Comment on: "On the relationship between induced polarization and surface conductivity: Implications for petrophysical interpretation of electrical measurements" (A. Weller, L. Slater, and S. Nordsiek, Geophysics, 78, no. 5, D315–D325): Geophysics, **79**, no. 2, X1–X5, doi: 10.1190/geo2013-0300.1.

Revil, A., A. Binley, L. Mejus, and P. Kessouri, 2015, Predicting permeability from the characteristic relaxation time and intrinsic formation factor of complex conductivity spectra: Water Resources Research, **51**, 6672–6700, doi: 10.1002/2015WR017074.

Revil, A., J. D. Eppehimer, M. Skold, M. Karaoulis, L. Godinez, and M. Prasad, 2013, Low-frequency complex conductivity of sandy and clayey materials: Journal of Colloid and Interface Science, **398**, 193–209, doi: 10.1016/j.jcis.2013.01.015.

Revil, A., N. Florsch, and D. Mao, 2015a, Induced polarization response of porous media with metallic particles. Part 1: A theory for disseminated semiconductors: Geophysics, **80**, no. 5, D525–D538, doi: 10.1190/geo2014-0577.1.

Revil, A., M. Karaoulis, T. Johnson, and A. Kemna, 2012, Review: Some low-frequency electrical methods for subsurface characterization and monitoring in hydrogeology: Hydrogeology Journal, **20**, 617–658, doi: 10.1007/s10040-011-0819-x.

Revil, A., G. Z. Abdel Aal, E. A. Atekwana, D. Mao, and N. Florsch, 2015b, Induced polarization response of porous media with metallic particles. Part 2: Comparison with a broad database of experimental data: Geophysics, **80**, no. 5, D539–D552, doi: 10.1190/geo2014-0578.1.

Revil, A., and N. Florsch, 2010, Determination of permeability from spectral induced polarization in granular media: Geophysical Journal International, **181**, 1480–1498, doi: 10.1111/j.1365-246X.2010.04573.x.

Revil, A., N. Florsch, and C. Camerlynck, 2014a, Spectral induced polarization porosimetry: Geophysical Journal International, **198**, 1016–1033, doi: 10.1093/gji/ggu180.

Revil, A., P. Kessouri, and C. Torres-Verdín, 2014b, Electrical conductivity, induced polarization, and permeability of the Fontainebleau sandstone: Geophysics, **79**, no. 5, D301–D318, doi: 10.1190/geo2014-0036.1.

Revil, A., and M. Skold, 2011, Salinity dependence of spectral induced polarization in sands and sandstones: Geophysical Journal International, **187**, 813–824, doi: 10.1111/gji.2011.187.issue-2.

Rink, M., and J. Schopper, 1974, Interface conductivity and its implications to electric logging: Presented at the SPWLA 15th Annual Logging Symposium, Paper J.

Schurr, J., 1964, On the theory of the dielectric dispersion of spherical colloidal particles in electrolyte solution: The Journal of Physical Chemistry, **68**, 2407–2413, doi: 10.1021/j100791a004.

Schwarz, G., 1962, A theory of the low-frequency dielectric dispersion of colloidal particles in electrolyte solution 1, 2: The Journal of Physical Chemistry, **66**, 2636–2642, doi: 10.1021/j100818a067.

Skold, M., A. Revil, and P. Vaudelet, 2011, The pH dependence of spectral induced polarization of silica sands: Experiment and modeling: Geophysical Research Letters, **38**, L12304, doi: 10.1029/2011GL047748.

Slater, L. D., and D. R. Glaser, 2003, Controls on induced polarization in sandy unconsolidated sediments and application to aquifer characterization: Geophysics, **68**, 1547–1558, doi: 10.1190/1.1620628.

van Olphen, H., and M. Waxman, 1958, Surface conductance of sodium bentonite in water: Proceedings of the 5th National Conference, Clays and Clay Minerals, NAS-RRC Pub. 566, 61–80.

Vaudelet, P., A. Revil, M. Schmutz, M. Franceschi, and P. Bégassat, 2011, Induced polarization signatures of cations exhibiting differential sorption behaviors in saturated sands: Water Resources Research, **47**, W02526, doi: 10.1029/2010WR009310.

Vinegar, H. J., and M. H. Waxman, 1984, Induced polarization of shaly sands: Geophysics, **49**, 1267–1287, doi: 10.1190/1.1441755.

Volkmann, J., and N. Klitzsch, 2016, Evaluation of low frequency polarization models using well characterized sintered porous glass samples: Journal of Applied Geophysics, **124**, 39–53, doi: 10.1016/j.jappgeo.2015.11.011.

Volkmann, J., N. Klitzsch, O. Mohnke, and N. Schleifer, 2013, Rock properties influencing impedance spectra (IS) studied by lab measurements on porous model systems: Proceedings of the International Symposium of the Society of Core Analysts, 419–424.

Weller, A., K. Breede, L. Slater, and S. Nordsiek, 2011, Effect of changing water salinity on complex conductivity spectra of sandstones: Geophysics, **76**, no. 5, F315–F327, doi: 10.1190/geo2011-0072.1.

Weller, A., and L. Slater, 2012, Salinity dependence of complex conductivity of unconsolidated and consolidated materials: Comparisons with electrical double layer models: Geophysics, **77**, no. 5, D185–D198, doi: 10.1190/geo2012-0030.1.

Weller, A., and L. Slater, 2015, Induced polarization dependence on pore space geometry: Empirical observations and mechanistic predictions: Journal of Applied Geophysics, **123**, 310–315, doi: 10.1016/j.jappgeo.2015.09.002.

Weller, A., L. Slater, J. A. Huisman, O. Esser, and F.-H. Haegel, 2015, On the specific polarizability of sands and sand-clay mixtures: Geophysics, **80**, no. 3, A57–A61, doi: 10.1190/geo2014-0509.1.

Weller, A., L. Slater, and S. Nordsiek, 2013, On the relationship between induced polarization and surface conductivity: Implications for petrophysical interpretation of electrical measurements: Geophysics, **78**, no. 5, D315–D325, doi: 10.1190/geo2013-0076.1.

Weller, A., L. Slater, and S. Nordsiek, 2014, Reply to discussion comment on: "On the relationship between induced polarization and surface conductivity: Implications for petrophysical interpretation of electrical measurements" (A. Weller, L. Slater, and S. Nordsiek, Geophysics, 78, no. 5, D315–D325): Geophysics, **79**, no. 2, X5–X10.

Weller, A., L. Slater, S. Nordsiek, and D. Ntarlagiannis, 2010, On the estimation of specific surface per unit pore volume from induced polarization: A robust empirical relation fits multiple data sets: Geophysics, **75**, no. 4, WA105–WA112, doi: 10.1190/1.3471577.

Zimmermann, E., A. Kemna, J. Berwix, W. Glaas, H. Münch, and J. Huisman, 2008, A high-accuracy impedance spectrometer for measuring sediments with low polarizability: Measurement Science and Technology, **19**, 105603, doi: 10.1088/0957-0233/19/10/105603.